Comparative study of a new structure of HTS-bulk axial flux-switching machine

Nima Arish[a] , Fabrizio Marignetti[b,*] , Mohammad Yazdani-Asrami

[a] Department of Electrical and Computer Engineering, Semnan University, Semnan, Iran
[b] Department of Electrical and Information Engineering the University of Cassino and South Lazio, Cassino, Italy
[c] Department of Electronic and Electrical Engineering, University of Strathclyde, Glasgow, U.K

[*]marignetti@unicas.it

Abstract: A high-temperature superconducting (HTS) axial flux permanent magnet (AFPM) machine was designed, using superconducting bulks over the rotor surface and rare-earth magnets in the middle of the stator teeth. Because of diamagnetic behavior of the HTS bulks and zero field cooling, leakage flux significantly reduces in the proposed machine compared to the existing machine with mounting rare-earth magnets. Three-dimensional finite element (FE) modelling was used to validate the design performance. The magnetic flux distribution, induced electromotive force (EMF), inductance, PM flux, losses, total harmonic distribution and cogging torque are computed and compared in two structures. The results show that the proposed machine structure is more efficient than the existing one.

1. Introduction

The axial flux permanent magnet machines (AFPMs) exhibit many advantages compared to other more conventional structures such as robust structure, low cogging torque, adjustable air gap, lighter weight, fault tolerance capability, higher efficiency and torque/power density [1-3]. Although, these machines suffer from unavoidable issues such as fabrication difficulties, demagnetization and high manufacturing cost. The literature reports various types of AFPMs, based on different principles, often using special materials for improving the performances. The soft magnetic composite (SMC), due to the low eddy currents loss, is a practical way to solve thermal problems, although their permeability is low and the hysteresis loss is higher. Authors in [4-6] used a SMC core to improve the performance of the machines in terms of thermal behavior. Also using HTS materials, can improve the performance of AFPMs, because of their high conductivity and flux trapping capability. HTS is applied in electric machines as Bulks [7, 8], Coils [9, 10], Tapes [11, 12], Magnets [13] and hybrid [14] for reducing leakage flux and magnetic saturation as well as increasing the overall electric load. Superconductors can be divided into two main categories: Type-I and type-II. The type-I superconductors lose their superconductivity very easily or suddenly when exposed to external magnetic fields. In superconducting state, this type of superconductors are completely diamagnetic. This phenomenon is known as the Meissner effect and it means magnetic susceptibility is equal to -1 [15, 16]. Type II superconductors such as BSCCO, YBCO, and GdBCO lose its superconductivity phase only if very intense fields are applied. Fig. 1 illustrates the operation of superconductor materials in all states. As can be seen, the type I superconductor after H_C completely will become the normal conductor and lose shielding feature. On the other hand, type II after H_{c1} lose shielding feature gradually and turn into normal conductor after H_{c2}. Using type-II superconductors as bulk in electric machine construction can reduce flux leakage and improve the magnetic flux distribution, which further increase both power density and efficiency of machine [17-19]. Recently, some innovative structures of axial flux-switching permanent magnet machines (AFSPMMs) were developed to provide very high torque-densities [20, 21]. Starting from these structures, this paper presents a superconducting HTS axial flux-switching machine (AFSM) using the HTS-Bulk among the rotor poles and also, rare-earth permanent magnets (PMs) in the middle of the stator teeth, resulting in a acceptable improvement in its performances. The rest of the paper is organized as follows: in Section 2, the topology of the proposed HTS AFSM, its operation principle and cooling system will be discussed. Section 3 is dedicated to using the FE modeling for machine performance analysis and discussions on the results.

2. Proposed Machine Topology and Operation

The structures of the existing AFSPMMs [20, 21] and the proposed HTS AFSM are shown in Fig. 2. The existing AFSPMM is a doubly salient machine with circumferentially magnetized PMs placed in the middle of the stator teeth. The salient rotor poles shunt the flux paths, providing the EMF in the stator windings.
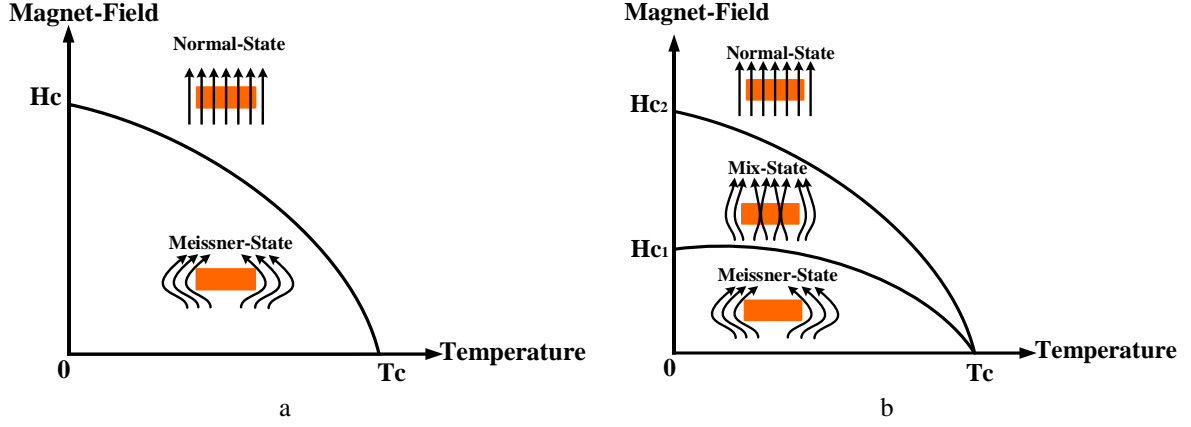
Fig. 1. Superconducting state. (a) Type I, (b) Type II.

To reduce the axial length and the rotor inertia, the saliency of the rotor is limited in the axial-flux machines. Exploiting the flux-shielding property of HTS-Bulk YBCO used between two consecutive rotor teeth, helps to increase the saliency and performance. The compared machines have a same dimensions, one rotor and one stator with the three-phase concentrated winding located on the stator as illustrated in Fig. 3. The main idea is that shielding the flux reduces the leakage and increases the reluctance ratio. Regardless of the stator resistance and leakage inductance the apparent power of an electric machine is given by [22]:

$$s_n = \varepsilon \frac{P_{in}}{\cos(\varphi)} \tag{1}$$

where P_{in} is the load input power, $\cos(\varphi)$ is the power factor, ϵ is the ratio of the EMF induced by the rotor E_{ph} and the excitation flux at no load V_{ph} :

$$\varepsilon = \frac{E_{ph}}{V_{ph}} = \begin{cases} Motor, & \varepsilon \prec 1 \\ Generator, & \varepsilon \succ 1 \end{cases} \tag{2}$$

with $\epsilon < 1$ in motoring operation and $\epsilon > 1$ in generator operation. The output power for both models can be calculated as:

$$P_{Out} = \frac{m}{T} \eta \int_0^T e_{ph}(t) i_s(t) dt = \frac{m}{2} \eta e_{ph} I_a \tag{3}$$

where T is the period of one EMF cycle, m is the number of machine phases, η is the efficiency, $e_{ph}(t)$ is the phase induced EMF, $i_s(t)$ is the phase current, e_{ph} is the peak value of the phase induced EMF and I_a is the peak value of the phase current. The maximum value of phase induced EMF for a generic flux-switching machine can be obtained by:

$$e_{ph} = N_{stage} N_{ph} \phi_{max} N_r \omega \tag{4}$$
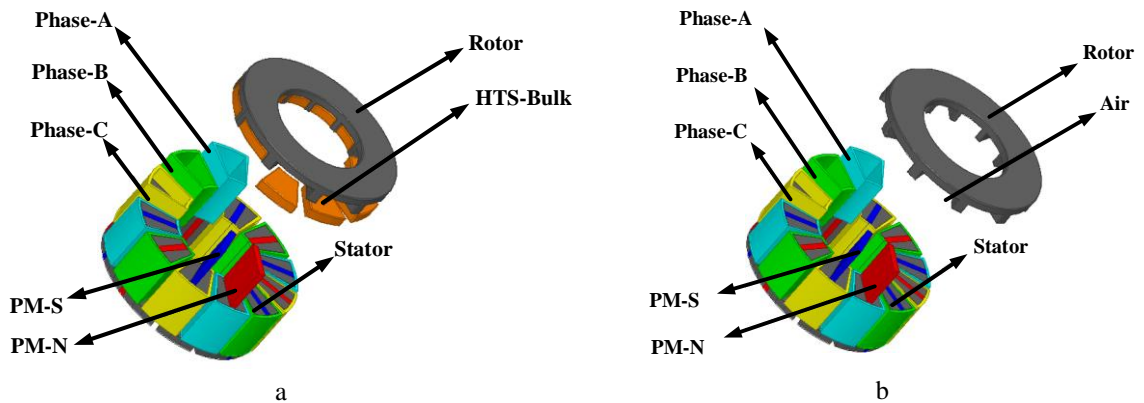
Fig. 2. Comparison of machine structures. (a) The proposed HTS AFSM, (b) The existing AFSPMM.
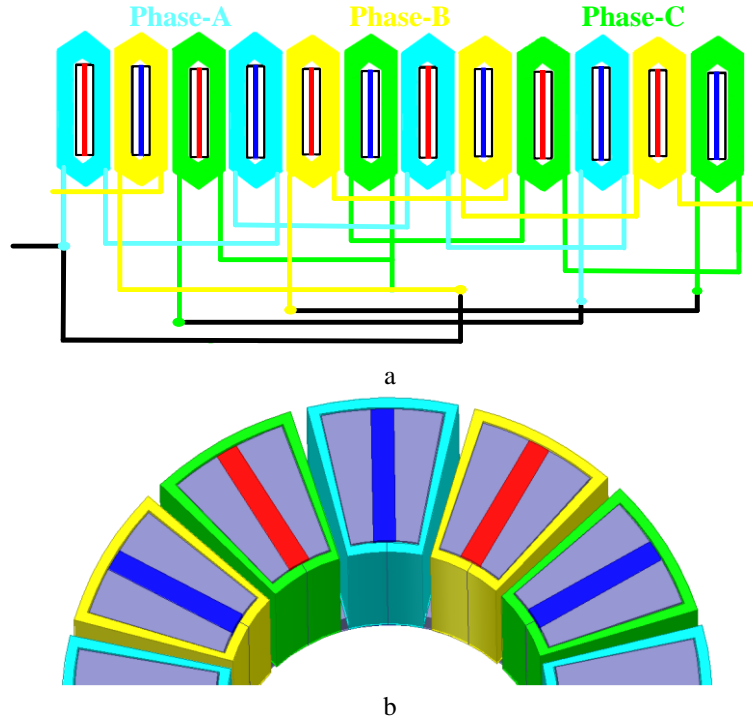
Fig. 3. Winding arrangement. (a) Winding connections, (b) Stator layout schematic.

where N_r is the rotor pole number, ω is the angular speed of the rotor, N_{st} is the number of machine stages, N_{ph} is the number of stator turns per phase per stator, ϕ_{max} is the phase PM flux per turn which can be computed as:

$$\phi_{max} = K_L K_F C_S B_G \frac{1}{N_S} \frac{\pi}{4} (1-k_d^2) D_{out}^2 \tag{5}$$

where N_s is the number of stator teeth, K_L is the leakage flux factor, K_F is the air-gap flux density distribution factor, C_S is the pole arc coefficient, B_g is the air gap flux density (average value), D_{out} is the outer diameter and k_d is the diameter ratio. The latter is an important design parameter which has a remarkable impact on the performance of the machine and is defined as:

$$k_d = \frac{D_{in}}{D_{out}} \tag{6}$$

To optimize the torque density of the machine, the value of K_d has to be selected carefully. The definitions of the design dimensions of the proposed HTS AFSM are illustrated in Fig. 4 and the design specifications are written in Table 1.

Table 1
Design specifications of the AFSPMM and the HTS AFSM.

Design data	Unite	Initial
Pout	KW	1
g	mm	1
Rate of speed	rpm	750
Current	A	8
Number of coil turns	-	184
Stator outer diameter	mm	182
Stator inner diameter	mm	100
Coil span	mm	6.5
l_{pm}	mm	6.5
l_{yr}	mm	8.3
l_{pr}	mm	12.5
l_{slot}	mm	57.5
l_{st}	mm	14.5
w_{coil}	mm	12
l_{pw}	mm	10
l_{ys}	mm	9.2

3
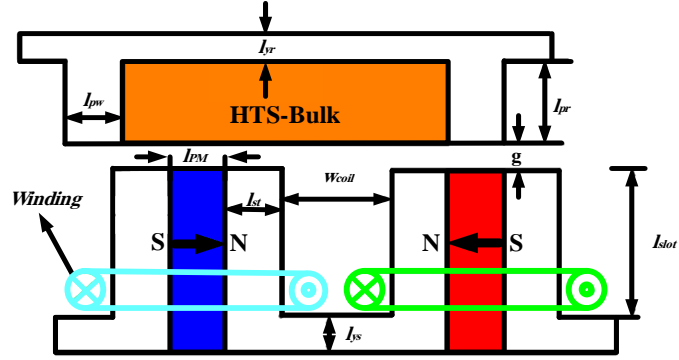
Fig. 4. Design dimensions of proposed HTS AFSM.

It should be noted that, cooling is very vital factor, as HTS-Bulks keep this unique feature of flux shielding only at very low temperature at below 77 K. There are two main methods for the cooling HTS-Bulk. Cooling before placing the HTS-Bulk in the rotor slot by helium vapors [23, 24] or cooling the HTS-Bulk after placing HTS-Bulk in the rotor slot by liquid nitrogen (LN2) [25, 26]. It is crucial to keep PMs away from the LN2, because if PMs are cooled to below 135 K their magnetization will no longer be uniaxial [27]. Therefore, the cooling system with a multi-layer damper tube or super insulation is considered for PMs avoid direct contact with the LN2 and HTS-Bulk [25, 26]. Fig. 5 shows conceptual cooling system of proposed HTS AFSM. The cooler pipe is mounted along the HTS bulks in the rotor and LN2 is realized and circulated by cooler pipe for reducing temperature at around 77 k to ensure that the HTS-bulks work properly. Considering the rotating movement of the rotor, the cooler pipes should be connected to the cooling system by the soft tube to tolerate rotor vibration.

3. FE modelling, simulation results and discussions

Due to the two-dimensional FE method does not yield satisfactory accuracy in computations for axial flux machines, especially in the case of high saturation levels, as usually happens for flux-switching machines, the three-dimensional FE modeling is chosen by Maxwell Ansys software. However, the three-dimensional FE method is time-consuming but necessary to achieve accurate analysis. The mesh for the proposed HTS AFSM is shown in Fig. 6. All properties, full geometric explanations and macroscopic behavior can be considered and applied to the superconducting material using non-linear resistivity which is related to the local current and defined as power-law [28]:

formulation uses the magnetic vector potential A $(B = \nabla \times A)$ and the electric scalar potential V. The electric field is expressed as:

$$E = -\frac{\partial A}{\partial t} - \nabla V \qquad (14)$$

and the equation to be solved is Ampere's law:

$$\nabla \times \frac{1}{\mu_0} \nabla \times A + \sigma \left(\frac{\partial A}{\partial t} + \nabla V \right) = 0 \qquad (15)$$

In the superconducting regions, σ is a non-linear conductivity describing the transition from superconducting to normal state. These regions are described by a non-linear resistivity derived by the power-law $E - J$ relation:

$$\rho(E) = \frac{E_c^{1/n}}{J_c} |E|^{(n-1)/n} + \rho_0 \qquad (16)$$

$$\vec{E}(T, \vec{B}, \vec{J}) = \frac{E_c}{J_c} \left| \frac{\vec{j}}{j_c} \right|^{n-1} \vec{J} \qquad (7)$$

where J_c is critical current density and E_c is the critical electrical field of superconductor. Maxwell's equation and (7) can be formulated in diversity of formulation namely A-V, T-Ω, E and H formulations. These formulas are basically the same, but the solutions for the relevant partial differential equation (PDE) are different by finite element [29, 30]. Maxwell Ansys software solve these equation as A-V method [31].
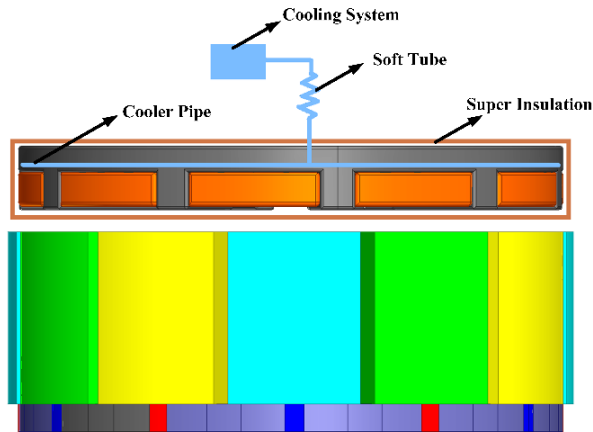

Fig. 5. Conceptual cooling system of proposed HTS AFSM.
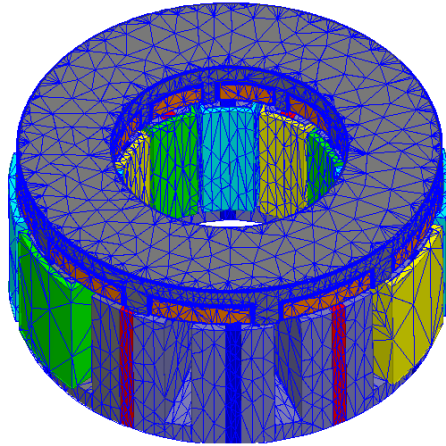
Fig. 6. Mesh operation for the proposed HTS AFSM (three coils are removed to show the slots mesh).

3.1. Magnetic flux-density distribution

Both models were simulated at the same condition. The only difference between the AFSPMM and HTS AFSM is the Bulk-HTS YBCO, which is located in the slot of the rotor. PMs and coils at full load state produce field density distribution. The magnetic field distribution of both machines at full load is shown in Fig. 7 and compared at the same speed and conditions. The peak of magnetic field in the two structures is fewer than 2 T, which, according to Fig. 7, suggests that the iron is not saturated and is still in the standard range and saturation effect in the HTS AFSM is lower than AFSPMM and, so the, magnetic reluctance is very high and does not allow the flux to penetrate in the HTS-Bulk.


a

b
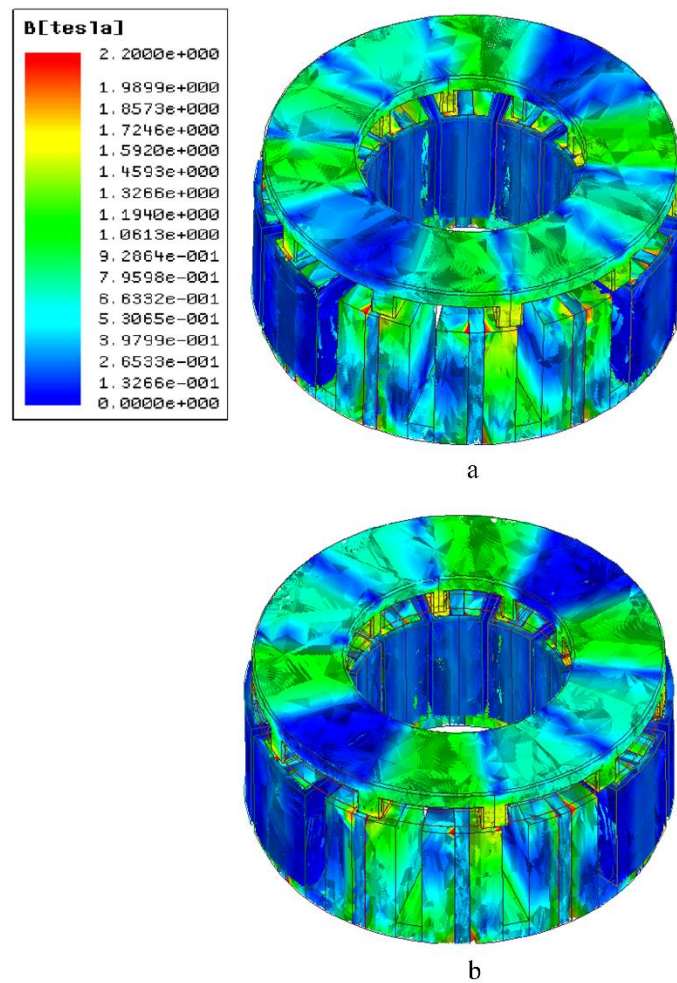
Fig. 7. Magnetic field distribution for both models. (a) Existing AFSPMM, (b) Proposed HTS AFSM.

Fig. 8 shows the flux-lines of the proposed HTS AFSM and the existing AFSPMM at no load and full load conditions. As can be seen, not only HTS-Bulk reduced leakage flux, but also protected flux linkage at the no load and full load states. The magnetic circuit for the leakage flux contour was modeled in Fig. 9. Leakage flux path of two machines can be given by:

$$\phi_{leakage} = \frac{F_m}{R_{PM} + R_x} \tag{8}$$

where R_x and F_m are the variable magnetic reluctance and magneto motive force (MMF) respectively and R_{PM} is the magnetic reluctance of the PM. According to Eq.(8), if R_x is assumed as a magnetic reluctance of HTS, because of the very low relative permeability of the HTS-Bulk, the magnetic reluctance of the HTS is extreme, which makes a significant reduction in leakage flux. Also, when R_x is assumed as a magnetic reluctance of airgap because the relative permeability of the air is higher than HTS the leakage flux in the proposed machine is lower than in the existing machine.
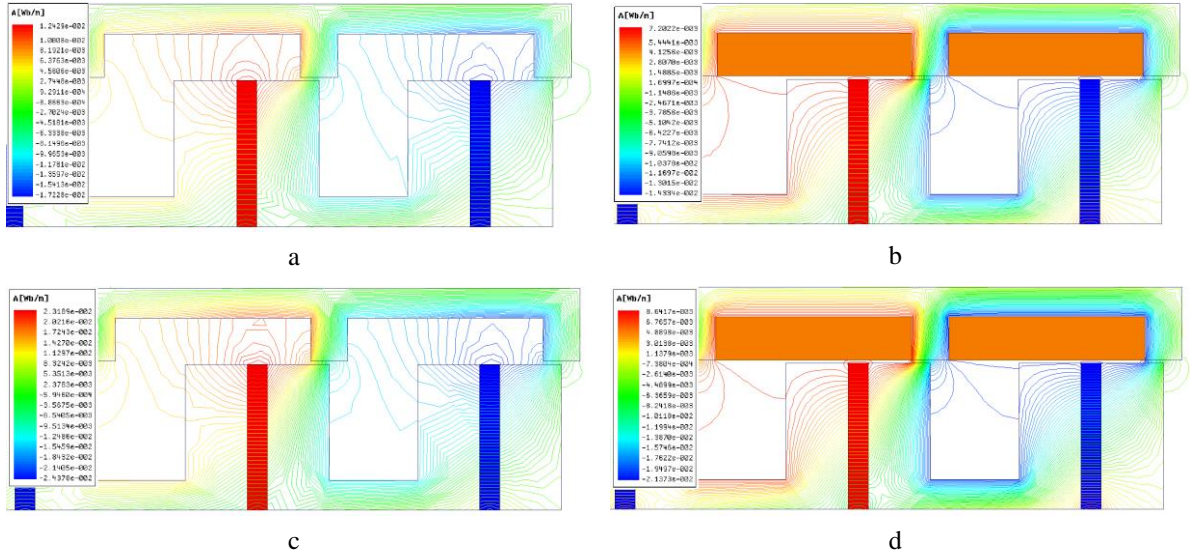
Fig. 8. Magnetic flux-lines distribution. (a) No-load state for existing AFSPMM, (b) No-load state for the proposed HTS AFSM, (c) Full-load state for existing AFSPMM, (d) Full-load state for the proposed HTS AFSM.
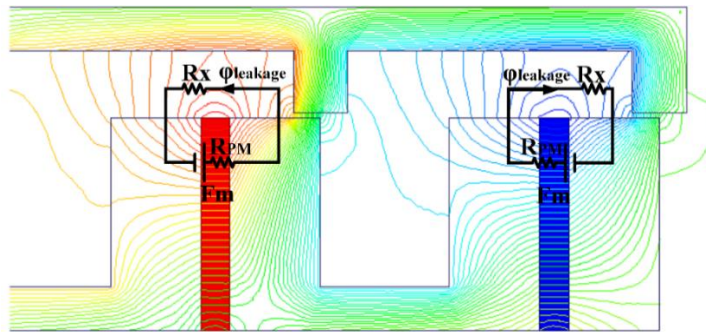
Fig. 9. The model of magnetic circuit for leakage flux contour.

3.2. Induced EMF and rotor flux-density

Fig. 10 illustrates the induced EMF of all coils belonging to the same phase in a mechanical period of 36 degrees. It can be concluded that the induced EMF in the HTS AFSM is higher than in the AFSPMM and the maximum value of the voltage is 81 V and 74 V, respectively. This increase is due to the decrease of leakage flux in the air gap. It is important to note that the induced voltage is the derivation of the PMs flux and these are proportional to each other, so that the magnetic flux increases as the induced voltage increases. Utilizing HTS-Bulk in the HTS AFSM makes total harmonic distribution (THD) diminish because THD depends on the geometry of the structure and adding HTS-Bulk changes air gap of the rotor's slot and the magnetic reluctance of machine.

The THD of EMF in the HTS AFSM and AFSPMM are 0.074 and 0.25, respectively. Fig. 11 compares the THD of EMF in the HTS AFSM and the AFSPMM. PM flux for both models is compared in Fig. 12 and it is obviously clear that the peak of PM flux in the HTS AFSM is higher than in the AFSPMM machine. The RMS values of PM flux for the HTS AFSM and the AFSPMM are 0.069 Wb and 0.047 Wb, respectively.

3.3. Self and mutual inductances

The quantity of self-inductance is related to the rotor position and the kind of coil, which has a considerable effect on the performance of the electrical machine. Since, the relative permeability of HTS-Bulk is lower than air [32], the effective air gap increases and as a result, the self-inductance reduces. The self-inductance value for each structure is shown in Fig. 13. The average self-inductances in the HTS AFSM and the AFSPMM are 4 mH and 4.9 mH respectively. The quantity of mutual-inductance for both structures is almost -2 mH which is shown in Fig. 14.

3.4. Cogging torque

Cogging torque is one of the fundamental concerns of any electrical machine design, as it has a remarkable impact on the performance of the electrical machine. Noise and vibration in electric PM machines have been created by high cogging torque [33]. Cogging torque in PM machine is due to the interaction between the magnets and the teeth. There are many ways to reduce cogging torque such as: correct selection of air gap, thickness of the magnets and teeth [34]. Fig. 16 shows the cogging torque for both models. As can be seen, the cogging torque in the proposed HTS AFSM is a little lower than AFSPMM, because by mounting HTS-Bulk the air gap of the slot of the rotor is reduced. The peak-to-peak value of the cogging torque for the HTS AFSM and the AFSPMM is 6.16 N and 6.36 N, respectively.
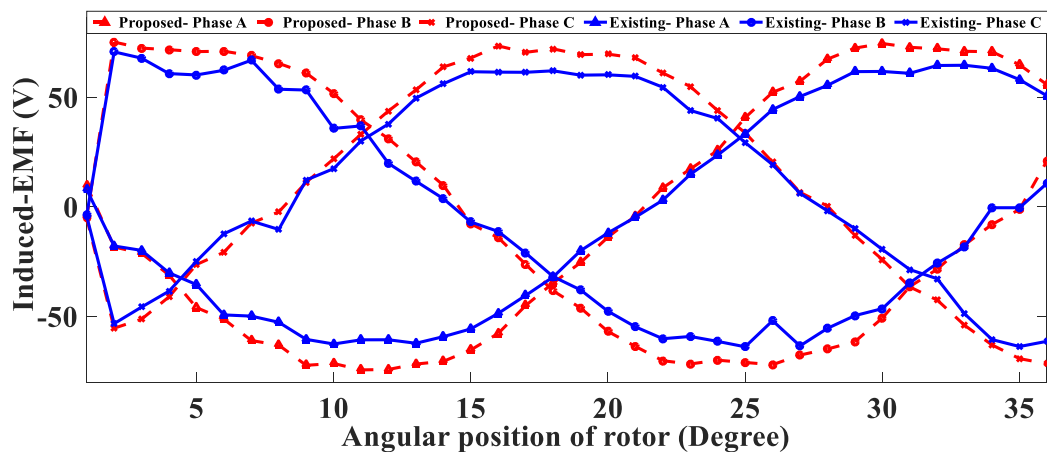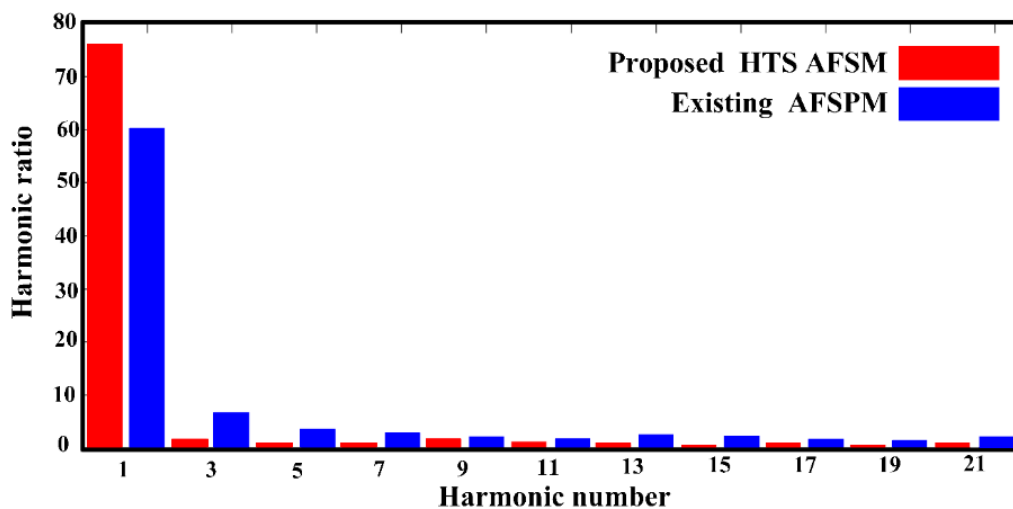

Fig. 10. Comparison of EMF for both models.

Fig. 11. Comparison of the EMF harmonic spectra for both models.
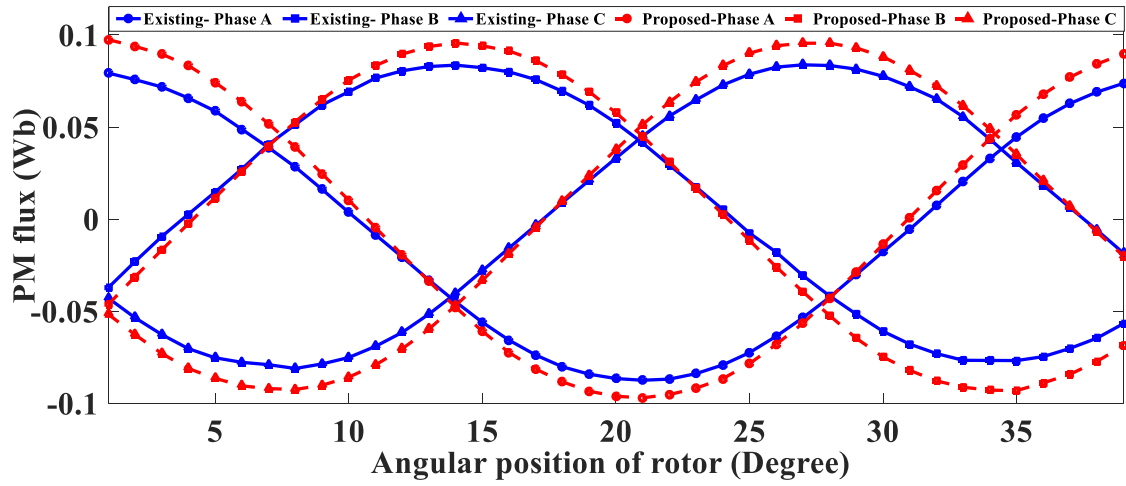
8

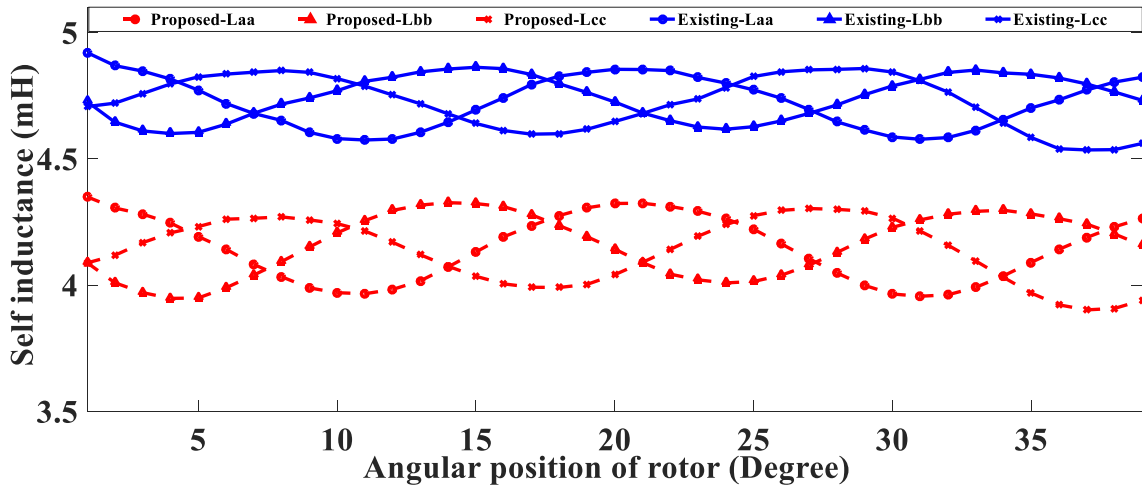**Fig. 12.** Comparison of PM flux for both models.

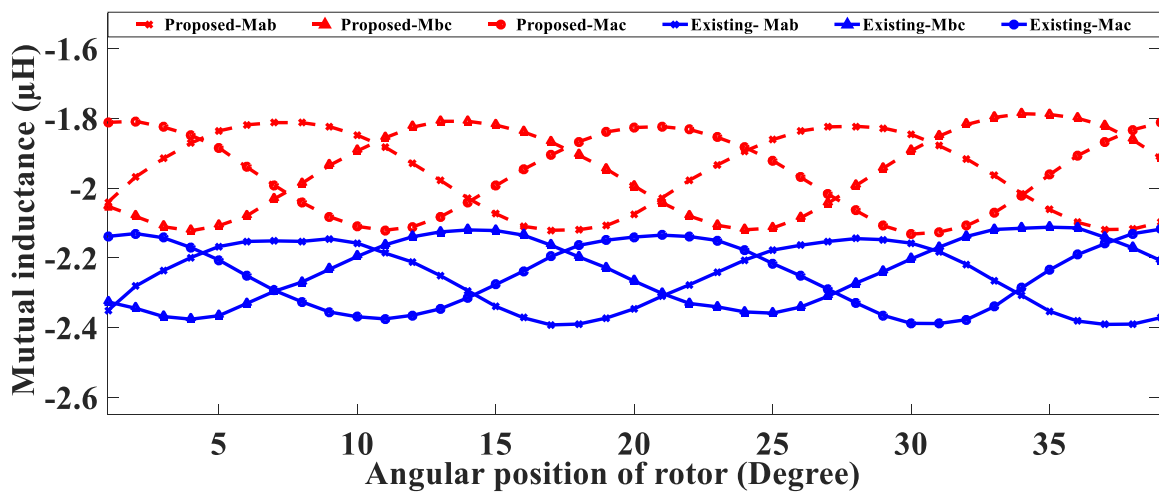**Fig. 13.** Comparison of self-inductance for both models.

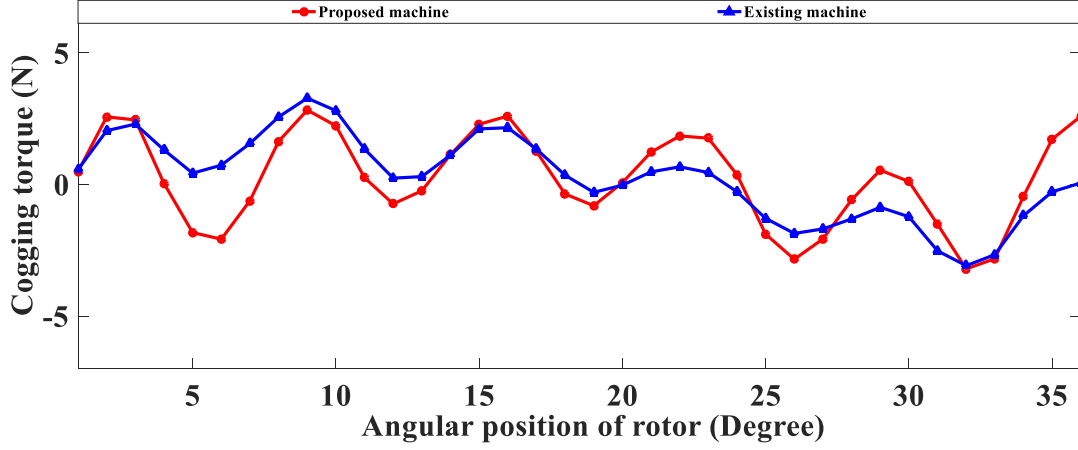**Fig. 14.** Comparison of mutual-inductance for both models.

Fig. 15. Comparison of cogging torque for both models.

3.5. Loss comparison

Losses in the back cores of both machines can be computed as follows [35]:

$$P_{loss} = nB^{1.6}f^{1.6} + KB^2f^2 \qquad (8)$$

where P_{loss} is the total loss, n is the hysteresis coefficient, B is the magnetic flux density, K is the eddy current loss factor and f is the frequency. When losses increase, the performance of the machine such as efficiency and cooling worsen. Higher losses consequently will increase heat production, especially in the coils, and if the cooling system cannot coup with this extra heat load effectively, it will cause a temperature change in superconducting material, and result in running the risk of a possible quench. Eddy and hysteresis losses are undesirable, so by reducing them, the machine performance improves. In PM electric machines, a major part of eddy losses is due to slot effects and space harmonics. Also, the reaction of the armature and the time harmonics are the main reasons for the heating and demagnetization of the magnets. The comparison of total loss for both models is in Fig. 16. It is clear that total loss for both machines is approximately the same. To achieve a better comparison and a fair analysis, all investigations of main parameters were made in the same condition and are shown in Tab. 2.
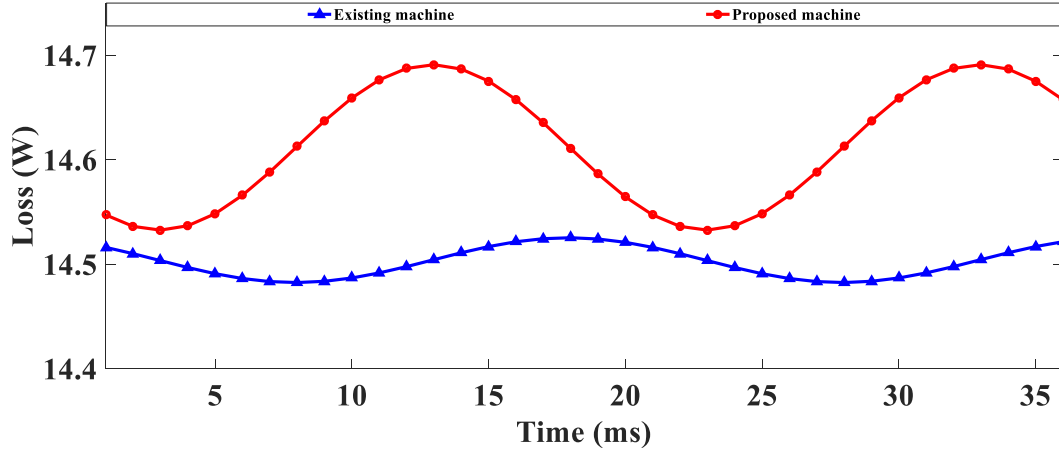

Fig. 16. Comparison of loss for both models.

Table 2
Performance comparison of the AFSPMM and the HTS AFSM.

Items	Unit	Proposed AFPM	Existing AFPM
PM flux	Wb	0.069	0.047
Induced-EMF	V	81	74
Inductance	mH	4	4.9
Cogging torque	N	6.16	6.36
Loss	W	14.17	14.15
THD	-	0.074	0.25

10

4. Conclusion

In this paper, a new structure for an axial flux-switching machine was proposed and compared with existing machine. The main novelty of the proposed machine is the use of HTS-Bulk YBCO. The YBCO material is located between the slots of the rotor as a bulk and circumferentially-magnetized rare-earth magnets are located inside the stator teeth. A significant reduction in leakage flux was achieved in the proposed machine because of zero field cooling and diamagnetic behavior of the HTS bulks. This unique feature forbids the flux to penetrate into the HTS-Bulk and therefore the air-gap leakage flux reduces while linkage flux in the yoke increases. The results of the FE modeling analyses demonstrate that the proposed HTS AFSM has a better performance compared to existing AFPM. The induced voltage and PM flux increase, while the inductance and cogging torque values reduce. Moreover, utilizing HTS-Bulk YBCO decreases the THD and magnetic saturation of the proposed machine. RMS of PM flux for proposed HTS AFSM and existing AFPM is 0.069 Wb and 0.047 Wb, respectively. The peak value of induced EMF for proposed HTS AFSM and existing AFPM is 81 V and 74V, respectively. The average self-inductance for proposed HTS AFSM and existing AFPM is 4 mH and 4.9 mH, respectively. The peak to peak value of cogging torque for proposed HTS AFSM and existing AFPM is 6.16 N and 6.36 N, respectively.

Reference

[1]   E. Hoang, A.H. Ben-Ahmed, and J. Lucidarme, Switching Flux Permanent Magnet Poly-Phased Synchronous Machines, in: Proceeding 7th Eur. Conf. Power Electron. Appl., 1997. doi:10.1109/63.575679.

[2]   W. Zhao, M. Cheng, K.T. Chau, J. Ji, W. Hua, R. Cao, A new modular flux-switching permanent-magnet machine using fault-tolerant teeth, in: Dig. 2010 14th Bienn. IEEE Conf. Electromagn. F. Comput. CEFC 2010, 2010. doi:10.1109/CEFC.2010.5481434.

[3]   Z.Q. Zhu, Y. Pang, D. Howe, S. Iwasaki, R. Deodhar, A. Pride, Analysis of electromagnetic performance of flux-switching permanent-magnet machines by nonlinear adaptive lumped parameter magnetic circuit model, IEEE Trans. Magn. (2005). doi:10.1109/TMAG.2005.854441.

[4]   F. Marignetti, V. Delli Colli, Y. Coia, Design of axial flux PM synchronous machines through 3-D coupled electromagnetic thermal and fluid-dynamical finite-element analysis, IEEE Trans. Ind. Electron. (2008). doi:10.1109/TIE.2008.2005017.

[5]   C.W. Kim, G.H. Jang, J.M. Kim, J.H. Ahn, C.H. Baek, J.Y. Choi, Comparison of Axial Flux Permanent Magnet Synchronous Machines with Electrical Steel Core and Soft Magnetic Composite Core, IEEE Trans. Magn. (2017). doi:10.1109/TMAG.2017.2701792.

[6]   Y. Wang, J. Lu, C. Liu, G. Lei, Y. Guo, J. Zhu, Development of a high-performance axial flux pm machine with smc cores for electric vehicle application, IEEE Trans. Magn. (2019). doi:10.1109/TMAG.2019.2914493.

[7]   M. Ardestani, N. Arish, H. Yaghobi, A new HTS dual stator linear permanent magnet Vernier machine with Halbach array for wave energy conversion, Phys. C Supercond. Its Appl. (2020). doi:10.1016/j.physc.2019.1353593.

[8]   N. Arish, Electromagnetic performance analysis of linear vernier machine with PM and HTS-Bulk, Phys. C Supercond. Its Appl. (2020). doi.org/10.1016/j.physc.2020.1353751

[9]   P.J. Masson, M. Breschi, P. Tixador, C.A. Luongo, Design of HTS axial flux motor for aircraft propulsion, in: IEEE Trans. Appl. Supercond., 2007. doi:10.1109/TASC.2007.898120.

[10]   Y. Wang, M. Chen, T.W. Ching, K.T. Chau, Design and analysis of a new HTS axial-field flux-switching machine, IEEE Trans. Appl. Supercond. (2015). doi:10.1109/TASC.2014.2366465.

[11]   G. Messina, M. Yazdani-Asrami, F. Marignetti, A. Della Corte, Characterization of HTS Coils for Superconducting Rotating Electric Machine Applications: Challenges, Material Selection, Winding Process, and Testing, IEEE Trans. Appl. Supercond. (2021). doi:10.1109/TASC.2020.3042829.

[12]   N. Arish, M. Ardestani, A. Hekmati, Optimum Structure of Rotor Slot for a 20 kW HTS Induction Motor, Phys. C Supercond. Its Appl. (2021).

[13]   M. Yazdani-Asrami, M. Zhang, W. Yuan, Challenges for developing high temperature superconducting

ring magnets for rotating electric machine applications in future electric aircrafts, J. Magn. Magn. Mater. (2021). doi:10.1016/j.jmmm.2020.167543.

[14]   A. Colle, T. Lubin, S. Ayat, O. Gosselin, J. Leveque, Analytical Model for the Magnetic Field Distribution in a Flux Modulation Superconducting Machine, IEEE Trans. Magn. (2019). doi:10.1109/TMAG.2019.2935696.

[15]   P. Tixador, P. Gautier-Picard, X. Chaud, Electrical motor with bulk Y-Ba-Cu-O pellets, IEEE Trans. Appl. Supercond. (1997). doi:10.1109/77.614648.

[16]   J. López, J. Lloberas, R. Maynou, X. Granados, R. Bosch, X. Obradorsand, R. Torres, AC three-phase axial flux motor with magnetized superconductors, in: IEEE Trans. Appl. Supercond., 2007. doi:10.1109/TASC.2007.898361.

[17]   M. Fee, M.P. Staines, R.G. Buckley, P.A. Watterson, J.G. Zhu, Calculation of AC loss in an HTS wind turbine generator, in: IEEE Trans. Appl. Supercond., 2003. doi:10.1109/TASC.2003.813032.

[18]   M.D. Ainslie, Y. Jiang, W. Xian, Z. Hong, W. Yuan, R. Pei, T.J. Flack, T.A. Coombs, Numerical analysis and finite element modelling of an HTS synchronous motor, in: Phys. C Supercond. Its Appl., 2010. doi:10.1016/j.physc.2010.05.200.

[19]   D.U. Gubser, Superconducting motors and generators for naval applications, in: Phys. C Supercond. Its Appl., 2003. doi:10.1016/S0921-4534(03)01124-9.doi:10.1109/TASC.2014.2357761.

[20]   J.H. Kim, Y. Li, B. Sarlioglu, Novel Six-Slot Four-Pole Axial Flux-Switching Permanent Magnet Machine for Electric Vehicle, IEEE Trans. Transp. Electrif. (2017). doi:10.1109/TTE.2016.2620169.

[21]   J.H. Kim, Y. Li, B. Sarlioglu, Design, analysis, and prototyping of axial flux-switching permanent magnet machine, in: 2017 IEEE Int. Electr. Mach. Drives Conf. IEMDC 2017, 2017. doi:10.1109/IEMDC.2017.8002272.

[22]   F. Marignetti, M.A. Darmani, S.M. Mirimani, Electromagnetic sizing of axial-field flux switching permanent magnet machine, in: IECON Proc. Industrial Electron. Conf., 2016. doi:10.1109/IECON.2016.7793175..

[23]   B. Felder, M. Miki, Z. Deng, K. Tsuzuki, N. Shinohara, M. Izumi, H. Hayakawa, Development of a cryogenic helium-neon gas mixture cooling system for use in a Gd-bulk HTS synchronous motor, IEEE Trans. Appl. Supercond. (2011). doi:10.1109/TASC.2010.2101573.

[24]   J. Bin Song, H. Lee, Mixed cryogen cooling systems for HTS power applications: A status report of progress in Korea University, in: Cryogenics (Guildf)., 2012. doi:10.1016/j.cryogenics.2012.06.013.

[25]   N. Baloch, S. Khaliq, B. Il Kwon, A High Force Density HTS Tubular Vernier Machine, IEEE Trans. Magn. (2017). doi:10.1109/TMAG.2017.2709339.

[26]   Y. Du, K.T. Chau, M. Cheng, Y. Fan, W. Zhao, F. Li, A linear stator permanent magnet vernier HTS machine for wave energy conversion, IEEE Trans. Appl. Supercond. 22 (2012). doi:10.1109/TASC.2012.2185473.

[27]   J. Li, K.T. Chau, A novel HTS PM vernier motor for direct-drive propulsion, IEEE Trans. Appl. Supercond. 21 (2011) 1175–1179. doi:10.1109/TASC.2010.2085412.

[28]   M. Yazdani-Asrami, S.A. Gholamian, S.M. Mirimani, J. Adabi, Investigation on Effect of Magnetic Field Dependency Coefficient of Critical Current Density on the AC Magnetizing Loss in HTS Tapes Exposed to External Field, J. Supercond. Nov. Magn. (2018). doi:10.1007/s10948-018-4664-1.

[29]   R. Shafaie, M. Kalantar, Comparison of theoretical and numerical electromagnetic modeling for HTS synchronous generator, IEEE Trans. Appl. Superconduct. 25 (2015) 1–7, doi:10.1109/TASC.2014.2357761.

[30]   M.D. Ainslie, H. Fujishiro, Modelling of bulk superconductor magnetization, Superconduct. Sci. Technol. 27 (2015) 053002. doi:10.1088/0953-2048/28/5/053002.

[31]   F. Grilli, R. Brambilla, L. Martini, Modeling high-temperature superconducting tapes by means of edge finite elements, IEEE Trans. Appl. Superconduct. 17 (2007) 3155–3158.

[32]   J. Jin, L. Zheng, W. Xu, Y. Guo, J. Zhu, Thrust characteristics of a double-sided high temperature superconducting linear synchronous motor with a high temperature superconducting magnetic suspension system, in: J. Appl. Phys., 2011. doi:10.1063/1.3572237.

[33] C.D. Botha, M.J. Kamper, R.J. Wang, A.J. Sorgdrager, Force ripple and cogging force minimisation criteria of single-sided consequent-pole linear vernier hybrid machines, in: Proc. - 2020 Int. Conf. Electr. Mach. ICEM 2020, 2020. doi:10.1109/ICEM49940.2020.9270845.

[34] S. Gerber, R.J. Wang, Cogging Torque Definitions for Magnetic Gears and Magnetically Geared Electrical Machines, IEEE Trans. Magn. (2018). doi:10.1109/TMAG.2017.2784823.

[35] I.C. Vese, F. Marignetti, M.M. Radulescu, Multiphysics approach to numerical modeling of a permanent-magnet tubular linear motor, IEEE Trans. Ind. Electron. (2010). doi:10.1109/TIE.2009.2030206.